Emergent Correlated Phases in Rhombohedral Trilayer Graphene Induced by Proximity Spin-Orbit and Exchange Coupling

Yaroslav Zhumagulov,[1,*] Denis Kochan,[2,1,3,†] and Jaroslav Fabian[1,‡]
[1]Institute for Theoretical Physics, University of Regensburg, 93040 Regensburg, Germany
[2]Institute of Physics, Slovak Academy of Sciences, 84511 Bratislava, Slovakia
[3]Center for Quantum Frontiers of Research and Technology (QFort), National Cheng Kung University, Tainan 70101, Taiwan

(Received 25 May 2023; revised 28 November 2023; accepted 22 March 2024; published 1 May 2024)

The impact of proximity-induced spin-orbit and exchange coupling on the correlated phase diagram of rhombohedral trilayer graphene (RTG) is investigated theoretically. By employing *ab initio*-fitted effective models of RTG encapsulated by transition metal dichalcogenides (spin-orbit proximity effect) and ferromagnetic $Cr_2Ge_2Te_6$ (exchange proximity effect), we incorporate the Coulomb interactions within the random-phase approximation to explore potential correlated phases at different displacement fields and doping. We find a rich spectrum of spin-valley resolved Stoner and intervalley coherence instabilities induced by the spin-orbit proximity effects, such as the emergence of a spin-valley-coherent phase due to the presence of valley-Zeeman coupling. Similarly, proximity exchange removes the phase degeneracies by biasing the spin direction, enabling a magnetocorrelation effect—strong sensitivity of the correlated phases to the relative magnetization orientations (parallel or antiparallel) of the encapsulating ferromagnetic layers.

DOI: 10.1103/PhysRevLett.132.186401

Introduction.—The discovery of correlated phases and superconductivity in magic-angle twisted bilayer graphene [1–4], which exhibits a highly flat band structure at the Fermi level [5–15], has prompted intense theoretical [16–26] and experimental [27–41] investigations. However, while the twist angle has emerged as a new tuning knob of the electronic properties of van der Waals heterostructures, it remains a challenge to control the stacking angle and limit twist disorder [42–49].

As shown recently, correlation phenomena are not exclusive to moiré structures. Observations of half and quarter metallic states [50–55] and superconductivity [52,56–65] in rhombohedral trilayer graphene (RTG), and of isospin magnetism and spin-polarized superconductivity in Bernal bilayer graphene [63–74], have demonstrated that rich physics of strong electronic correlations can be manifested in more conventional, moiré-less graphene systems. The key feature shared by magic-angle twisted bilayer graphene with Bernal-stacked bilayer graphene and RTG is the presence of pronounced van Hove singularities (vHSs) in the electronic density of states near the charge neutrality point [5,6,75]. In RTG, the low energy of a vHS allows tuning the induced symmetry-breaking phases by doping [50], while its multilayered atomic structure enables efficient control of the vHS and thus correlated phases via a displacement field [50,75]. This tunability makes RTG a promising platform for exploring strongly correlated physics.

Electronic band structures can also be tuned by van der Waals engineering. In particular, proximity-induced spin interactions—spin-orbit (SO) and exchange (EX) couplings—can furnish graphene with what it lacks: SO fields and spin polarization. Indeed, proximity-induced SO and EX interactions in graphene-based heterostructures have been theoretically predicted [76–88] and experimentally observed [89–100], demonstrating the appearance of valley-Zeeman, Kane-Mele, and Rashba SO coupling [76–83,89–99] as well as (anti)ferromagnetic EX couplings [80,81,83–85,87,99–101] on the meV scale. It should be possible to swap SO and EX couplings via a displacement field [80,81].

It is natural to ask what effects can arise from combining correlated physics and proximity-induced spin interactions. Concerning RTG, two observations are crucial: (i) The vHSs are formed by the bands comprising the top and bottom layer p_z orbitals, and (ii) the spin proximity effects are on the meV scale, which is also expected for the correlated band gaps. The above suggests that spin proximity effects can significantly alter symmetry-broken phases in RTG.

In this Letter, we demonstrate that, indeed, proximity SO and EX interactions induce and control novel strongly correlated phases. Specifically, we study $MoSe_2$/RTG/WSe_2 heterostructures for the SO proximity effect, and CGT/RTG/CGT heterostructures with parallel and antiparallel magnetizations of CGT ($Cr_2Ge_2Te_6$) for the EX proximity effect [83], see Fig. 1(a). Employing the random-phase approximation (RPA) [102–107], we first calculate the correlated phase diagram of pristine RTG, which exhibits either an intervalley coherent (IVC) state [108] or a Stoner instability, as already predicted [59,60]. The spin interactions remove the degeneracies of IVC and Stoner phases by introducing spin anisotropy and spin bias. Novel phases, such as a spin-valley-coherent (SVC)

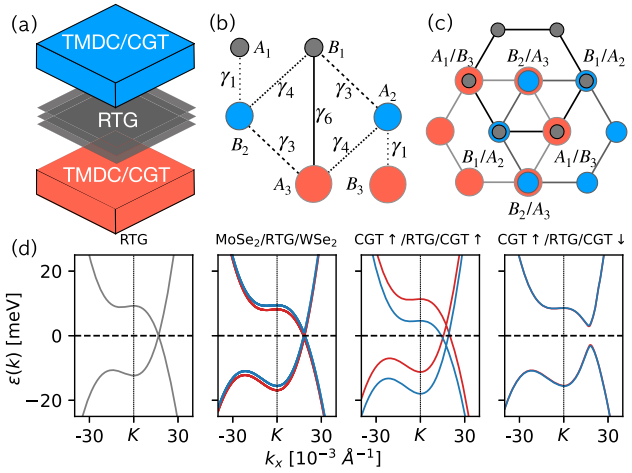

FIG. 1. (a) Scheme of an RTG-based heterostructure encapsulated by transition-metal dichalcogenide (TMDC) or CGT monolayers, which induce, respectively, SO or EX interactions in RTG. (b) RTG unit cell with the relevant interlayer orbital hoppings γ. The colors distinguish the three layers and A_l and B_l denote sublattice sites of the lth layer. (c) The top-down view of the RTG lattice. (d) Calculated single-particle low-energy electronic dispersions at K for pristine RTG and indicated heterostructures (red marks spin-up and blue spin-down states).

state, arise primarily due to proximity-induced valley-Zeeman coupling; Rashba coupling plays a lesser role. The SVC phase opens new avenues for spintronics [109] since the Coulomb interactions induce novel spin-valley couplings. Finally, the magnetic heterostructures exhibit a strong magnetocorrelation effect—the induced phases are sensitive to the relative orientation of the CGT magnetizations.

Model.—We model the orbital physics of proximitized RTG by a realistic hopping Hamiltonian [75,83,110–112]:

$$\hat{h}_0 = \begin{pmatrix} u_d & \gamma_0 f & \gamma_4 f^* & \gamma_1 & 0 & 0 \\ \gamma_0 f^* & \eta + u_d & \gamma_3 f & \gamma_4 f^* & \gamma_6 & 0 \\ \gamma_4 f & \gamma_3 f^* & u_m & \gamma_0 f & \gamma_4 f^* & \gamma_1 \\ \gamma_1 & \gamma_4 f & \gamma_0 f^* & u_m & \gamma_3 f & \gamma_4 f^* \\ 0 & \gamma_6 & \gamma_4 f & \gamma_3 f^* & \eta - u_d & \gamma_0 f \\ 0 & 0 & \gamma_1 & \gamma_4 f & \gamma_0 f^* & -u_d \end{pmatrix} \quad (1)$$

acting on single-particle Bloch states with momenta $\mathbf{k} = (k_x, k_y)$—measured from K and K' valleys—that are based on carbon p_z-orbital orbitals residing on the RTG sublattices (A_1, B_1, A_2, B_2, A_3, B_3). Here, $f = -(\sqrt{3}a/2)(\tau k_x - i k_y)$ is the linearized nearest-neighbor structure factor, a is graphene's lattice constant, and $\tau_{K/K'} = \pm 1$ is the valley index; γ_i are orbital hopping parameters, see Fig. 1(b). The unit cell and lattice structure of RTG are shown in Figs. 1(b) and 1(c). The electrostatic potentials on different layers are incorporated into Eq. (1) through the different on-site energies u_d, u_m, and $-u_d$, such that $2u_d$ corresponds to the potential energy difference between the external layers due to an applied displacement field. Finally, η is the on-site potential applied to those sites which are hybridized via the vertical γ_6 hopping, see Fig. 1(b).

Pristine RTG exhibits weak SO coupling at K and K' valleys, on the scale of 10 μeV [110,112]. Thus, we consider RTG encapsulated by strong SO materials $MoSe_2$ and WSe_2, and by ferromagnetic CGT; as shown by *ab initio* simulations, they induce spin splittings on the 1 meV scale [83]. The corresponding proximity-induced SO and EX coupling Hamiltonian $\hat{h}_{\rm prox} = \sum_l \hat{h}^l_R + \hat{h}^l_I + \hat{h}^l_{\rm ex}$ of RTG electrons is the sum of Rashba, $\hat{h}^l_R$, intrinsic, $\hat{h}^l_I$, and exchange, $\hat{h}^l_{\rm ex}$, terms in the given lth layer [79,82,83,86], parameterized, correspondingly, by the sublattice-resolved couplings λ^l_R, λ^{A_l/B_l}_I and $\lambda^{A_l/B_l}_{\rm ex}$:

$$\hat{h}^l_R + \hat{h}^l_I + \hat{h}^l_{\rm ex} = \begin{pmatrix} (\tau\lambda^{A_l}_I - \lambda^{A_l}_{\rm ex}) s_z & 2i\lambda^l_R s^\tau_- \\ -2i\lambda^l_R s^\tau_+ & -(\tau\lambda^{B_l}_I + \lambda^{B_l}_{\rm ex}) s_z \end{pmatrix}. \quad (2)$$

Here $s_{x,y,z}$ are the Pauli matrices acting on spin degrees of freedom and $s^\tau_\pm = \frac{1}{2}(s_x \pm i\tau s_y)$ are the valley-resolved spin-flip operators. Each $\hat{h}^l$ is 4×4 matrix in the spin-sublattice resolved $(A_{l\uparrow}, A_{l\downarrow}, B_{l\uparrow}, B_{l\downarrow})$ Bloch basis valid near the K/K' valleys. Since the proximity effects in van der Waals stacks are appreciable only in the layers closest to the proximitizing substrates [here transition-metal dichalcogenides (TMDCs)]—as shown by first-principles calculations [83]—it is sufficient to consider the spin Hamiltonian only in the two outer layers. Spin-orbit coupling in graphene induced by TMDCs is of the valley-Zeeman type [78], meaning that $\lambda^{A_l}_I \approx -\lambda^{B_l}_I$.

The numerical values for the parameters of the Hamiltonian $\hat{h}(\mathbf{k}, \tau) = \hat{h}_0 + \hat{h}_{\rm prox}$ are taken from the *ab initio* results of Ref. [83]. The calculated low-energy band dispersions for pristine RTG, $MoSe_2$/RTG/WSe_2, and CGT/RTG/CGT with both parallel and antiparallel CGT magnetizations are shown in Fig. 1(d).

We describe the correlation effects in RTG by Hamiltonian $\hat{H} = \hat{H}_{\rm kin} + \hat{H}_{\rm int}$,

$$\hat{H}_{\rm kin} = \sum_{\mathbf{k}\tau, si, s'j} [\hat{h}(\mathbf{k}, \tau) - \mu\hat{I}]_{si,s'j} \hat{c}^\dagger_{s\tau i}(\mathbf{k}) \hat{c}_{s'\tau j}(\mathbf{k}), \quad (3)$$

$$\hat{H}_{\rm int} = U(n_{\uparrow K} n_{\downarrow K} + n_{\uparrow K'} n_{\downarrow K'}) + V n_K n_{K'}, \quad (4)$$

where μ stands for the chemical potential and $\hat{c}^{(\dagger)}_{s\tau i}(\mathbf{k})$ is the annihilation (creation) operator for a Bloch electron with spin $s = \uparrow/\downarrow$ in valley $\tau = K/K'$ on RTG sublattice i with a valley-momentum $\mathbf{k}$. The intra- and intervalley density interactions are described by repulsive (positive) couplings U and V, respectively, while $n_{s\tau} = \sum_{|\mathbf{k}|<\Lambda} \sum_i \hat{c}^\dagger_{s\tau i}(\mathbf{k}) \hat{c}_{s\tau i}(\mathbf{k})$

TABLE I. List of spin-valley resolved symmetry-broken phases of RTG and their corresponding phase-ordering operators: $\hat{\Phi} = \sum_{|\mathbf{k}|<\Lambda} \sum_i \hat{c}^\dagger_{s\tau i}(\mathbf{k})[M_\Phi]_{s\tau,s'\tau'}\hat{c}_{s'\tau' i}(\mathbf{k}) = \hat{\Phi}^\dagger$, the underlying matrices M_Φ entering $\hat{\Phi}$'s are given in the third line. Phases descending from the Stoner phase preserve the translational symmetry of graphene, while the phases originating from the IVC break it. All correlated phases break time-reversal symmetry.

Pristine RTG phases	IVC		Stoner		
Proximity-induced phases	$\mathrm{VC}_\pm$	$\mathrm{SVC}_\pm$	$\mathrm{SVP}_\pm$	$\mathrm{VP}_\pm$	$\mathrm{SP}_\pm$
Spin-valley order operators M_Φ	$[s_0 \pm s_z]\tau_x$	$s_x\tau_x \pm s_y\tau_y$	$s_z\tau_0 \pm s_0\tau_z$	$[s_0 \pm s_z]\tau_z$	$s_{x/y}[\tau_0 \pm \tau_z]$

stands for a spin-valley number operator in the $s\tau$ channel cut off by momentum Λ; correspondingly $n_\tau = n_{\uparrow\tau} + n_{\downarrow\tau}$ stands for the valley-resolved number operator. Specifically, we consider SU(4)-symmetric interactions [59,113] by setting $U = V = 19$ eV, and $\Lambda = 0.06$ Å^{-1}, yielding the pristine RTG phase diagram consistent with experimental findings [50,56]. We use the same interaction parameters for the encapsulated cases as well. However, dielectric screening from the substrates may potentially affect the resulting phase diagrams on a quantitative, but not qualitative level.

Methodology.—To systematically determine the correlated phases of proximitized RTG we employ the RPA. For that, we first calculate the static noninteracting Lindhard's susceptibility χ^0 at 4.2 K projected [105–107,114] to different spin-valley channels employing the noninteracting Hamiltonian $\hat{H}_{\mathrm{kin}}$, Eq. (3). The RPA-corrected susceptibility equals $\chi = [1 - \chi^0\Gamma]^{-1}\chi^0$, where Γ is the fully irreducible vertex function [114] corresponding to $\hat{H}_{\mathrm{int}}$, Eq. (4). A correlated phase emerges if the highest eigenvalue λ_c of $\chi^0\Gamma$ becomes greater or equal to unity. Correspondingly, χ changes sign or diverges, indicating an emergence of instability that forces a system to undergo a phase transition.

We find all possible correlated phases $\hat{\Phi}$ (more precisely, the corresponding matrices M_Φ) by diagonalizing $\chi^0\Gamma$ at $\mu = 0$ and $u_d = 0$, i.e., for a charge neutral system without an external field. Only the phases $\hat{\Phi}$ as listed in Table I are relevant for our $MoSe_2$/RTG/WSe_2 and CGT/RTG/CGT heterostructure models. Then, we compute the corresponding χ^0 and $\chi^0\Gamma$ by varying doping and the displacement field. For each $\hat{\Phi}$ we calculate a critical parameter $\lambda_c^{\hat{\Phi}} = \langle\hat{\Phi}|\chi^0\Gamma|\hat{\Phi}\rangle/\|\hat{\Phi}\|^2$ that serves as a figure of merit for comparing and quantifying different instabilities. As the dominant instability we assign a phase $\hat{\Phi}$ that at given μ and u_d gives the maximal $\lambda_c^{\hat{\Phi}}$.

We first explore the correlated phase diagram of pristine RTG, shown in Fig. 2, featuring IVC ($M_\Phi \propto \tau_{x,y}$) and the Stoner ($M_\Phi \propto \tau_z$) instabilities, as also reported earlier [53,59,60]. While the Stoner instability is spatially local, an IVC state describes a spatially modulated phase with a wave vector $\mathbf{K}$ connecting K and K' valleys. As listed in Table I, the IVC and Stoner phases exhibit some degeneracies in the spin channel due to the high symmetry of pristine RTG as inherent to the SU(4) model.

Spin-orbit proximity effects.—We now turn to a $MoSe_2$/RTG/WSe_2 heterostructure model [80,81], which exemplifies the SO effects on the correlated physics. We consider here a generic set of SO parameters [83], which describe a zero twist-angle heterostructure.

The phase diagram in Fig. 3(a) displays differences from the case of pristine RTG. The Stoner phase separates into two spin-valley polarized states, $\mathrm{SVP}_\pm$, both spin polarized along the z direction in a way inherent to the form of single-particle valley-Zeeman coupling [78]. The degeneracy of the IVC phase is removed, resulting in spin-valley coherent and valley coherent states—$\mathrm{SVC}_\pm$ and $\mathrm{VC}_\pm$—with the resulting in-plane and out-of-plane spin polarization.

The $\mathrm{SVC}_\pm$ phases manifest at the electron doping near the vHS split by SO fields. As the corresponding $M_{\mathrm{SVC}_\pm} = s_x\tau_x \pm s_y\tau_y$ can be seen as a Coulomb interaction enabled intervalley spin-flip hopping that retains the spin-valley quantum number, i.e., the product of $s\tau$. $\mathrm{SVC}_\pm$ in-plane spin polarizations $\propto \cos(2\mathbf{K}\cdot\mathbf{R})s_x \pm \sin(2\mathbf{K}\cdot\mathbf{R})s_y$ resembling a Neél texture. At the same time, $\mathrm{VC}_\pm$ spin polarizations $\propto \cos(2\mathbf{K}\cdot\mathbf{R})[s_0 \pm s_z]$, i.e., they give an out-of-plane spin-wave-density modulation. An almost degenerate nature of $\mathrm{VC}_\pm$ phases is predicted, which separation largely depends on the model parameters due to the insignificant difference in the critical parameter $\lambda_c^{\hat{\Phi}}$.

We performed self-consistent calculations of the correlated band structure of $MoSe_2$/RTG/WSe_2 using the Hartree-Fock method [114]. Figures 3(b) and 3(c) show the correlated bands as Hartree-Fock excitation dispersions folded into the Γ point, as would be the case for a 3×3 unit

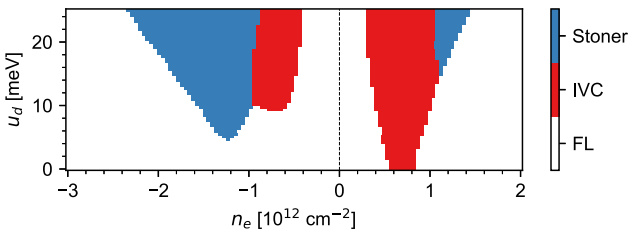

FIG. 2. Calculated phase diagram of pristine RTG ($\hat{h}_{\mathrm{prox}} = 0$) for varying doping n_e and displacement field u_d. There are two dominant phases: the intervalley coherent phase (IVC) and Stoner instability. The white background corresponds to a stable Fermi liquid (FL).

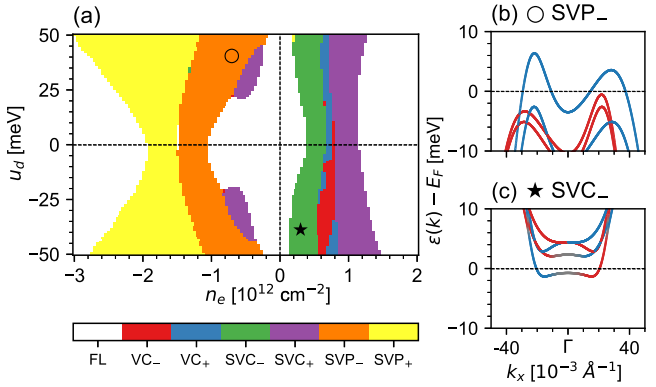

FIG. 3. (a) Calculated phase diagram of $MoSe_2/RTG/WSe_2$ heterostructure ($\hat{h}_R \neq 0$, $\hat{h}_I \neq 0$, and $\hat{h}_{\rm ex} = 0$) in the space spanned by displacement field u_d and doping density n_e. Six symmetry-breaking phases: $VC_\pm$ (valley coherent state), $SVC_\pm$ (spin-valley coherent state), and $SVP_\pm$ (spin-valley polarized state), marked by different colors, are predicted apart from the Fermi liquid state (white). Hartree-Fock excitation dispersions for (b) $u_d = 40$ meV and $n_e = -0.7 \times 10^{12}$ cm^{-2}, and (c) $u_d = -40$ meV and $n_e = 0.3 \times 10^{12}$ cm^{-2}. Red, blue, and gray lines mark spin-up, spin-down, and spin-unpolarized states.

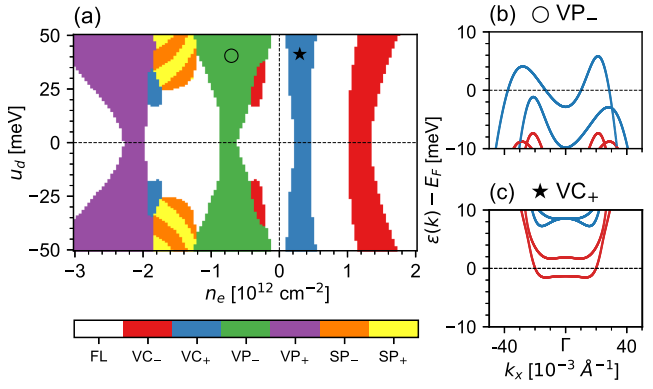

FIG. 4. (a) Calculated phase diagram of the CGT/RTG/CGT system with ferromagnetic CGT configuration ($\hat{h}_R = 0$, $\hat{h}_I = 0$, and $\hat{h}_{\rm ex} \neq 0$) in a parameter space spanned by displacement field u_d and electron doping n_e. Six symmetry broken phases, $VC_\pm$—valley coherent state, $VP_\pm$—valley-polarized state, and $SP_\pm$—in-plane spin-polarized state, are predicted and displayed by different colors, along with the Fermi liquid (FL) state. (b),(c) Correlated band structures of the CGT/RTG/CGT system for ferromagnetic CGT alignment at displacement field $u_d = 40$ meV with two different electron dopings: (b) $n_e = -0.7 \times 10^{12}$ cm^{-2} and (c) $n_e = 0.3 \times 10^{12}$ cm^{-2}. The color code represents spin expectation values: red for spin-up, blue for spin-down, and grey for spin-unpolarized.

cell. Panel (b) represents the correlation-modified electronic band structure of the SVP_- phase, while panel (c) displays the corresponding band structure of the SVC_- phase. We calculated the Hartree-Fock self-energy $\hat{\Sigma}$ corresponding to $\hat{H}_{\rm int}$, Eq. (4), and based on it, we estimated the correlated gaps, $\Delta_{\hat{\Phi}} = \sum_{s\tau,s'\tau'} \hat{\Phi}^*_{s'\tau',s\tau} \hat{\Sigma}_{s\tau,s'\tau'} / \|\hat{\Phi}\|^2$, which is comparable to the strength of the proximity-induced SO couplings, $\Delta_{\rm SVP\_} = 1.391$ meV and $\Delta_{\rm SVC\_} = 0.979$ meV. Therefore, by adding the term $\hat{H}_\Delta = \Delta_{\hat{\Phi}} \hat{\Phi}$ into the single-particle Hamiltonian $\hat{H}_{\rm kin}$, we can model an interacting system with a symmetry broken phase on a self-consistent mean-field level. The $SVC_\pm$ phase can be modeled by

$$\hat{H}_{\rm SVC_\pm} = \Delta_{\rm SVC_\pm} \sum_{\substack{i,\mathbf{k} \\ ss' \\ \tau\tau'}} [s_x\tau_x \pm s_y\tau_y]_{s\tau,s'\tau'} \hat{c}^\dagger_{s\tau i}(\mathbf{k}) \hat{c}_{s'\tau' i}(\mathbf{k}), \quad (5)$$

which effectively couples single-particle excitations with opposite spins and valleys. The SVC coupling should profoundly affect spintronics, potentially leading to novel spin relaxation mechanisms, spin-valley Hall effects, topological states, or even spin-valley qubits in confined structures. The above effective Hamiltonian allows one to study such phenomena already on the single-particle level.

Exchange proximity effects.—Encapsulating RTG by ferromagnetic CGT induces spin splitting of the RTG bands, depending on the relative magnetization orientation of the CGT layer (parallel or antiparallel). We adopt the zero-twist heterostructure model EX parameters [83].

The calculated CGT/RTG/CGT phase diagram with the parallel CGT magnetizations is shown in Fig. 4(a). The electron doping regime's $VC_\pm$ phase appears near the vHS. The Stoner phase is manifested in $VP_\pm$ and $SP_\pm$ states. The absence of the $SVC_\pm$ and $SVP_\pm$ phases can be accounted for by the lack of the spin-valley coupled physics due to the absence of the valley-Zeeman SO coupling. Similar to the $VC_\pm$ phase in MoSe2/RTG/WSe2, the SP_+ and SP_- phases exhibit close degeneracy, and their splitting strongly depends on the model parameters.

Using the Hartree-Fock method, we examined the emergent electronic band structure of the CGT/RTG/CGT heterostructure. Figure 4(b) shows the VP_- phase, and Fig. 4(c) presents the SVC_+ correlated band structure. The correlated gaps match EX coupling amplitudes, particularly, $\Delta_{\rm VP\_} = 1.408$ meV and $\Delta_{\rm SVC_+} = 0.771$ meV.

Finally, we calculated the CGT/RTG/CGT phase diagram with antiparallel CGT magnetizations, shown in Fig. 5(a). It exhibits strong tunability and displacement field asymmetry due to the contrasting magnetic order of the adjacent CGT layers. Similar to the ferromagnetic case, Stoner instability appears as $VP_\pm$ and $SP_\pm$ states mainly in a hole doping regime, while IVC as $VC_\pm$ states in an electron-doped one. Contrary to the ferromagnetic case, in the CGT/RTG/CGT heterostructure with antiferromagnetic CGT layer ordering, the sign of the displacement field strongly determines the $\pm$ sign of the underlying correlated states. Figures 5(b) and 5(c) display correlated Hartree-Fock electronic band structures for two specific correlated phases of antiferromagnetic CGT/RTG/CGT, VP_+ and SVC_+, respectively. Correlated gaps for these two cases

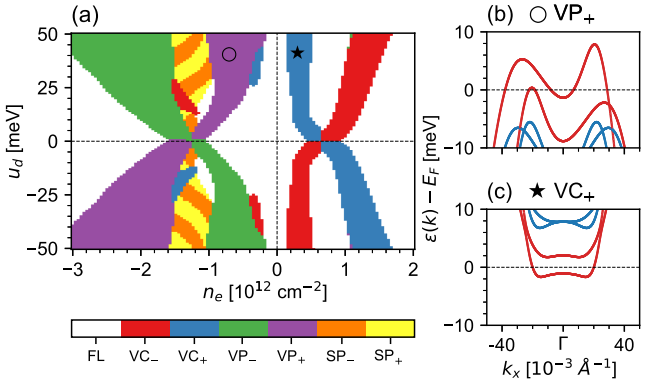

FIG. 5. (a) Phase diagram of the CGT/RTG/CGT electron system with antiferromagnetic CGT alignments ($\hat{h}_R = 0$, $\hat{h}_I = 0$, and $\hat{h}_{\rm ex} \neq 0$) in a parameter space of displacement field u_d and electron doping n_e. Six phases with symmetry breaking, $\mathrm{VC}_\pm$—valley coherent state, $\mathrm{VP}_\pm$—valley-polarized state, and $\mathrm{SP}_\pm$—in-plane spin-polarized state, are predicted along with the Fermi Liquid (FL) phase. (b), (c) Correlated band structure of the CGT/RTG/CGT system with antiferromagnetic CGT layers at displacement field $u_d = 40$ meV and electron doping level (b) $n_e = -0.7 \times 10^{12}$ cm^{-2} and (c) $n_e = 0.3 \times 10^{12}$ cm^{-2}. The color code represents spin expectation values: red for spin-up, blue for spin-down, and grey for spin-unpolarized.

are commensurate with EX coupling amplitudes and read $\Delta_{\mathrm{VP}_+} = 1.320$ meV and $\Delta_{\mathrm{SVC}_+} = 0.756$ meV.

Conclusion.—By performing realistic simulations of electronic correlations at the RPA and Hartree-Fock levels, we predict a strong interplay between proximity-induced SO and EX interactions and Coulomb-correlations of RTG. While we specifically consider $MoSe_2$/RTG/WSe_2 and CGT/RTG/CGT heterostructures, we expect our findings to be more generally applicable. The proposed emergence of spin-valley interactions facilitated by electronic correlations in the presence of SO coupling is particularly exciting, as it can enable new spintronic phenomena in van der Waals heterostructures. It is also expected that proximity spin interactions will affect superconducting correlations in RTG [56,60,61].

This work was funded by the Deutsche Forschungsgemeinschaft (DFG, German Research Foundation) SPP 2244 (Project No. 443416183), SFB 1277 (Project-ID 314695032), by the European Union Horizon 2020 Research and Innovation Program under Contract No. 881603 (Graphene Flagship), and by FLAG-ERA project 2DSOTECH. D. K. acknowledges partial support from the IMPULZ project IM-2021-26—SUPERSPIN funded by the Slovak Academy of Sciences. D. K. acknowledges partial support from the project IM-2021-26 (SUPERSPIN) funded by the Slovak Academy of Sciences via the program IMPULZ 2021 and Grant No. DESCOM VEGA 2/0183/21.

*iaroslav.zhumagulov@ur.de
†denis.kochan@savba.sk
‡jaroslav.fabian@ur.de

[1] C. R. Dean, L. Wang, P. Maher, C. Forsythe, F. Ghahari, Y. Gao, J. Katoch, M. Ishigami, P. Moon, M. Koshino, T. Taniguchi, K. Watanabe, K. L. Shepard, J. Hone, and P. Kim, Nature (London) **497**, 598 (2013).
[2] Y. Kim, P. Herlinger, P. Moon, M. Koshino, T. Taniguchi, K. Watanabe, and J. H. Smet, Nano Lett. **16**, 5053 (2016).
[3] Y. Cao, V. Fatemi, S. Fang, K. Watanabe, T. Taniguchi, E. Kaxiras, and P. Jarillo-Herrero, Nature (London) **556**, 43 (2018).
[4] Y. Cao, V. Fatemi, A. Demir, S. Fang, S. L. Tomarken, J. Y. Luo, J. D. Sanchez-Yamagishi, K. Watanabe, T. Taniguchi, E. Kaxiras, R. C. Ashoori, and P. Jarillo-Herrero, Nature (London) **556**, 80 (2018).
[5] G. Li, A. Luican, J. M. B. L. dos Santos, A. H. C. Neto, A. Reina, J. Kong, and E. Y. Andrei, Nat. Phys. **6**, 109 (2009).
[6] R. Bistritzer and A. H. MacDonald, Proc. Natl. Acad. Sci. U.S.A. **108**, 12233 (2011).
[7] I. Brihuega, P. Mallet, H. González-Herrero, G. Trambly de Laissardière, M. M. Ugeda, L. Magaud, J. M. Gómez-Rodríguez, F. Ynduráin, and J.-Y. Veuillen, Phys. Rev. Lett. **109**, 196802 (2012).
[8] L. A. Ponomarenko, R. V. Gorbachev, G. L. Yu, D. C. Elias, R. Jalil, A. A. Patel, A. Mishchenko, A. S. Mayorov, C. R. Woods, J. R. Wallbank, M. Mucha-Kruczynski, B. A. Piot, M. Potemski, I. V. Grigorieva, K. S. Novoselov, F. Guinea, V. I. Fal'ko, and A. K. Geim, Nature (London) **497**, 594 (2013).
[9] E. Suárez Morell, J. D. Correa, P. Vargas, M. Pacheco, and Z. Barticevic, Phys. Rev. B **82**, 121407(R) (2010).
[10] G. T. de Laissardière, D. Mayou, and L. Magaud, Nano Lett. **10**, 804 (2010).
[11] S. Shallcross, S. Sharma, E. Kandelaki, and O. A. Pankratov, Phys. Rev. B **81**, 165105 (2010).
[12] A. Luican, G. Li, A. Reina, J. Kong, R. R. Nair, K. S. Novoselov, A. K. Geim, and E. Y. Andrei, Phys. Rev. Lett. **106**, 126802 (2011).
[13] P. Moon and M. Koshino, Phys. Rev. B **85**, 195458 (2012).
[14] J. M. B. Lopes dos Santos, N. M. R. Peres, and A. H. Castro Neto, Phys. Rev. B **86**, 155449 (2012).
[15] J. M. B. Lopes dos Santos, N. M. R. Peres, and A. H. Castro Neto, Phys. Rev. Lett. **99**, 256802 (2007).
[16] G. Chaudhary, A. H. MacDonald, and M. R. Norman, Phys. Rev. Res. **3**, 033260 (2021).
[17] N. F. Q. Yuan and L. Fu, Phys. Rev. B **98**, 045103 (2018).
[18] L. Rademaker, I. V. Protopopov, and D. A. Abanin, Phys. Rev. Res. **2**, 033150 (2020).
[19] S. Javvaji, J.-H. Sun, and J. Jung, Phys. Rev. B **101**, 125411 (2020).
[20] H. C. Po, L. Zou, A. Vishwanath, and T. Senthil, Phys. Rev. X **8**, 031089 (2018).
[21] M. Xie and A. H. MacDonald, Phys. Rev. Lett. **124**, 097601 (2020).
[22] S. Carr, D. Massatt, S. Fang, P. Cazeaux, M. Luskin, and E. Kaxiras, Phys. Rev. B **95**, 075420 (2017).
[23] P. Potasz, M. Xie, and A. H. MacDonald, Phys. Rev. Lett. **127**, 147203 (2021).

[24] D. M. Kennes, J. Lischner, and C. Karrasch, Phys. Rev. B **98**, 241407(R) (2018).
[25] J. W. F. Venderbos and R. M. Fernandes, Phys. Rev. B **98**, 245103 (2018).
[26] F. Wu, E. Hwang, and S. Das Sarma, Phys. Rev. B **99**, 165112 (2019).
[27] M. Yankowitz, S. Chen, H. Polshyn, Y. Zhang, K. Watanabe, T. Taniguchi, D. Graf, A. F. Young, and C. R. Dean, Science **363**, 1059 (2019).
[28] X. Lu, P. Stepanov, W. Yang, M. Xie, M. A. Aamir, I. Das, C. Urgell, K. Watanabe, T. Taniguchi, G. Zhang, A. Bachtold, A. H. MacDonald, and D. K. Efetov, Nature (London) **574**, 653 (2019).
[29] Y. Xie, A. T. Pierce, J. M. Park, D. E. Parker, E. Khalaf, P. Ledwith, Y. Cao, S. H. Lee, S. Chen, P. R. Forrester, K. Watanabe, T. Taniguchi, A. Vishwanath, P. Jarillo-Herrero, and A. Yacoby, Nature (London) **600**, 439 (2021).
[30] G. W. Burg, J. Zhu, T. Taniguchi, K. Watanabe, A. H. MacDonald, and E. Tutuc, Phys. Rev. Lett. **123**, 197702 (2019).
[31] P. Rickhaus, F. K. de Vries, J. Zhu, E. Portoles, G. Zheng, M. Masseroni, A. Kurzmann, T. Taniguchi, K. Watanabe, A. H. MacDonald, T. Ihn, and K. Ensslin, Science **373**, 1257 (2021).
[32] Y. Choi, J. Kemmer, Y. Peng, A. Thomson, H. Arora, R. Polski, Y. Zhang, H. Ren, J. Alicea, G. Refael, F. von Oppen, K. Watanabe, T. Taniguchi, and S. Nadj-Perge, Nat. Phys. **15**, 1174 (2019).
[33] X. Liu, Z. Hao, E. Khalaf, J. Y. Lee, Y. Ronen, H. Yoo, D. H. Najafabadi, K. Watanabe, T. Taniguchi, A. Vishwanath, and P. Kim, Nature (London) **583**, 221 (2020).
[34] D. Wong, K. P. Nuckolls, M. Oh, B. Lian, Y. Xie, S. Jeon, K. Watanabe, T. Taniguchi, B. A. Bernevig, and A. Yazdani, Nature (London) **582**, 198 (2020).
[35] U. Zondiner, A. Rozen, D. Rodan-Legrain, Y. Cao, R. Queiroz, T. Taniguchi, K. Watanabe, Y. Oreg, F. von Oppen, A. Stern, E. Berg, P. Jarillo-Herrero, and S. Ilani, Nature (London) **582**, 203 (2020).
[36] A. Kerelsky, L. J. McGilly, D. M. Kennes, L. Xian, M. Yankowitz, S. Chen, K. Watanabe, T. Taniguchi, J. Hone, C. Dean, A. Rubio, and A. N. Pasupathy, Nature (London) **572**, 95 (2019).
[37] Y. Jiang, X. Lai, K. Watanabe, T. Taniguchi, K. Haule, J. Mao, and E. Y. Andrei, Nature (London) **573**, 91 (2019).
[38] H. Polshyn, M. Yankowitz, S. Chen, Y. Zhang, K. Watanabe, T. Taniguchi, C. R. Dean, and A. F. Young, Nat. Phys. **15**, 1011 (2019).
[39] I. Das, C. Shen, A. Jaoui, J. Herzog-Arbeitman, A. Chew, C.-W. Cho, K. Watanabe, T. Taniguchi, B. A. Piot, B. A. Bernevig, and D. K. Efetov, Phys. Rev. Lett. **128**, 217701 (2022).
[40] E. Codecido, Q. Wang, R. Koester, S. Che, H. Tian, R. Lv, S. Tran, K. Watanabe, T. Taniguchi, F. Zhang, M. Bockrath, and C. N. Lau, Sci. Adv. **5**, eaaw9770 (2019).
[41] L. Balents, C. R. Dean, D. K. Efetov, and A. F. Young, Nat. Phys. **16**, 725 (2020).
[42] T. E. Beechem, T. Ohta, B. Diaconescu, and J. T. Robinson, ACS Nano **8**, 1655 (2014).
[43] A. Uri, S. Grover, Y. Cao, J. A. Crosse, K. Bagani, D. Rodan-Legrain, Y. Myasoedov, K. Watanabe, T. Taniguchi, P. Moon, M. Koshino, P. Jarillo-Herrero, and E. Zeldov, Nature (London) **581**, 47 (2020).
[44] A. C. Gadelha, D. A. A. Ohlberg, F. C. Santana, G. S. N. Eliel, J. S. Lemos, V. Ornelas, D. Miranda, R. B. Nadas, K. Watanabe, T. Taniguchi, C. Rabelo, P. P. de Mello Venezuela, G. Medeiros-Ribeiro, A. Jorio, L. G. Cançado, and L. C. Campos, ACS Appl. Nano Mater. **4**, 1858 (2021).
[45] J. H. Wilson, Y. Fu, S. Das Sarma, and J. H. Pixley, Phys. Rev. Res. **2**, 023325 (2020).
[46] N. P. Kazmierczak, M. V. Winkle, C. Ophus, K. C. Bustillo, S. Carr, H. G. Brown, J. Ciston, T. Taniguchi, K. Watanabe, and D. K. Bediako, Nat. Mater. **20**, 956 (2021).
[47] N. Nakatsuji and M. Koshino, Phys. Rev. B **105**, 245408 (2022).
[48] R. Samajdar and M. S. Scheurer, Phys. Rev. B **102**, 064501 (2020).
[49] G. Shavit, K. Kolář, C. Mora, F. von Oppen, and Y. Oreg, Phys. Rev. B **107**, L081403 (2023).
[50] H. Zhou, T. Xie, A. Ghazaryan, T. Holder, J. R. Ehrets, E. M. Spanton, T. Taniguchi, K. Watanabe, E. Berg, M. Serbyn, and A. F. Young, Nature (London) **598**, 429 (2021).
[51] A. L. Szabó and B. Roy, Phys. Rev. B **105**, L081407 (2022).
[52] D.-C. Lu, T. Wang, S. Chatterjee, and Y.-Z. You, Phys. Rev. B **106**, 155115 (2022).
[53] C. Huang, T. M. R. Wolf, W. Qin, N. Wei, I. V. Blinov, and A. H. MacDonald, Phys. Rev. B **107**, L121405 (2023).
[54] F. Winterer, F. R. Geisenhof, N. Fernandez, A. M. Seiler, F. Zhang, and R. T. Weitz, arXiv:2305.04950.
[55] F. R. Geisenhof, F. Winterer, A. M. Seiler, J. Lenz, T. Xu, F. Zhang, and R. T. Weitz, Nature (London) **598**, 53 (2021).
[56] H. Zhou, T. Xie, T. Taniguchi, K. Watanabe, and A. F. Young, Nature (London) **598**, 434 (2021).
[57] Y.-Z. Chou, F. Wu, J. D. Sau, and S. Das Sarma, Phys. Rev. Lett. **127**, 187001 (2021).
[58] A. Ghazaryan, T. Holder, M. Serbyn, and E. Berg, Phys. Rev. Lett. **127**, 247001 (2021).
[59] Y.-Z. You and A. Vishwanath, Phys. Rev. B **105**, 134524 (2022).
[60] S. Chatterjee, T. Wang, E. Berg, and M. P. Zaletel, Nat. Commun. **13**, 6013 (2022).
[61] T. Cea, P. A. Pantaleón, V. T. Phong, and F. Guinea, Phys. Rev. B **105**, 075432 (2022).
[62] W. Qin, C. Huang, T. Wolf, N. Wei, I. Blinov, and A. H. MacDonald, Phys. Rev. Lett. **130**, 146001 (2023).
[63] A. Jimeno-Pozo, H. Sainz-Cruz, T. Cea, P. A. Pantaleón, and F. Guinea, Phys. Rev. B **107**, L161106 (2023).
[64] P. A. Pantaleón, A. Jimeno-Pozo, H. Sainz-Cruz, V. T. Phong, T. Cea, and F. Guinea, Nat. Rev. Phys. **5**, 304 (2023).
[65] Z. Li, X. Kuang, A. Jimeno-Pozo, H. Sainz-Cruz, Z. Zhan, S. Yuan, and F. Guinea, Phys. Rev. B **108**, 045404 (2023).
[66] H. Zhou, L. Holleis, Y. Saito, L. Cohen, W. Huynh, C. L. Patterson, F. Yang, T. Taniguchi, K. Watanabe, and A. F. Young, Science **375**, 774 (2022).
[67] Y. Zhang, R. Polski, A. Thomson, É. Lantagne-Hurtubise, C. Lewandowski, H. Zhou, K. Watanabe, T. Taniguchi,

J. Alicea, and S. Nadj-Perge, Nature (London) **613**, 268 (2023).
[68] A. M. Seiler, F. R. Geisenhof, F. Winterer, K. Watanabe, T. Taniguchi, T. Xu, F. Zhang, and R. T. Weitz, Nature (London) **608**, 298 (2022).
[69] Y.-Z. Chou, F. Wu, J. D. Sau, and S. Das Sarma, Phys. Rev. B **105**, L100503 (2022).
[70] S. C. de la Barrera, S. Aronson, Z. Zheng, K. Watanabe, T. Taniguchi, Q. Ma, P. Jarillo-Herrero, and R. Ashoori, Nat. Phys. **18**, 771 (2022).
[71] L. Holleis, C. L. Patterson, Y. Zhang, H. M. Yoo, H. Zhou, T. Taniguchi, K. Watanabe, S. Nadj-Perge, and A. F. Young, arXiv:2303.00742.
[72] A. L. Szabó and B. Roy, Phys. Rev. B **105**, L201107 (2022).
[73] Y.-Z. Chou, F. Wu, and S. Das Sarma, Phys. Rev. B **106**, L180502 (2022).
[74] Z. Dong, A. V. Chubukov, and L. Levitov, Phys. Rev. B **107**, 174512 (2023).
[75] F. Zhang, B. Sahu, H. Min, and A. H. MacDonald, Phys. Rev. B **82**, 035409 (2010).
[76] A. López, L. Colmenárez, M. Peralta, F. Mireles, and E. Medina, Phys. Rev. B **99**, 085411 (2019).
[77] T. Naimer, K. Zollner, M. Gmitra, and J. Fabian, Phys. Rev. B **104**, 195156 (2021).
[78] M. Gmitra and J. Fabian, Phys. Rev. B **92**, 155403 (2015).
[79] M. Gmitra, D. Kochan, P. Högl, and J. Fabian, Phys. Rev. B **93**, 155104 (2016).
[80] K. Zollner and J. Fabian, Phys. Rev. B **104**, 075126 (2021).
[81] K. Zollner, M. Gmitra, and J. Fabian, Phys. Rev. Lett. **125**, 196402 (2020).
[82] M. Gmitra, D. Kochan, and J. Fabian, Phys. Rev. Lett. **110**, 246602 (2013).
[83] K. Zollner, M. Gmitra, and J. Fabian, Phys. Rev. B **105**, 115126 (2022).
[84] K. Zollner, M. Gmitra, T. Frank, and J. Fabian, Phys. Rev. B **94**, 155441 (2016).
[85] H. Haugen, D. Huertas-Hernando, and A. Brataas, Phys. Rev. B **77**, 115406 (2008).
[86] D. Kochan, S. Irmer, and J. Fabian, Phys. Rev. B **95**, 165415 (2017).
[87] K. Zollner and J. Fabian, Phys. Rev. Lett. **128**, 106401 (2022).
[88] I. Žutić, A. Matos-Abiague, B. Scharf, H. Dery, and K. Belashchenko, Mater. Today **22**, 85 (2019).
[89] J. H. Garcia, M. Vila, A. W. Cummings, and S. Roche, Chem. Soc. Rev. **47**, 3359 (2018).
[90] J. O. Island, X. Cui, C. Lewandowski, J. Y. Khoo, E. M. Spanton, H. Zhou, D. Rhodes, J. C. Hone, T. Taniguchi, K. Watanabe, L. S. Levitov, M. P. Zaletel, and A. F. Young, Nature (London) **571**, 85 (2019).
[91] A. M. Hoque, D. Khokhriakov, K. Zollner, B. Zhao, B. Karpiak, J. Fabian, and S. P. Dash, Commun. Phys. **4**, 124 (2021).
[92] T. S. Ghiasi, J. Ingla-Aynés, A. A. Kaverzin, and B. J. van Wees, Nano Lett. **17**, 7528 (2017).
[93] T. S. Ghiasi, A. A. Kaverzin, P. J. Blah, and B. J. Van Wees, Nano Lett. **19**, 5959 (2019).
[94] C. K. Safeer, J. Ingla-Aynés, F. Herling, J. H. Garcia, M. Vila, N. Ontoso, M. R. Calvo, S. Roche, L. E. Hueso, and F. Casanova, Nano Lett. **19**, 1074 (2019).
[95] F. Herling, C. K. Safeer, J. Ingla-Aynés, N. Ontoso, L. E. Hueso, and F. Casanova, APL Mater. **8**, 071103 (2020).
[96] T. Wakamura, F. Reale, P. Palczynski, M. Q. Zhao, A. T. C. Johnson, S. Guéron, C. Mattevi, A. Ouerghi, and H. Bouchiat, Phys. Rev. B **99**, 245402 (2019).
[97] T. Wakamura, N. J. Wu, A. D. Chepelianskii, S. Guéron, M. Och, M. Ferrier, T. Taniguchi, K. Watanabe, C. Mattevi, and H. Bouchiat, Phys. Rev. Lett. **125**, 266801 (2020).
[98] J. Ingla-Aynés, F. Herling, J. Fabian, L. E. Hueso, and F. Casanova, Phys. Rev. Lett. **127**, 047202 (2021).
[99] A. A. Kaverzin, T. S. Ghiasi, A. H. Dismukes, X. Roy, and B. J. van Wees, 2D Mater. **9**, 045003 (2022).
[100] B. Karpiak, A. W. Cummings, K. Zollner, M. Vila, D. Khokhriakov, A. M. Hoque, A. Dankert, P. Svedlindh, J. Fabian, S. Roche, and S. P. Dash, 2D Mater. **7**, 015026 (2019).
[101] M. Peralta, E. Medina, and F. Mireles, Phys. Rev. B **99**, 195452 (2019).
[102] D. Bohm and D. Pines, Phys. Rev. **82**, 625 (1951).
[103] D. Pines and D. Bohm, Phys. Rev. **85**, 338 (1952).
[104] D. Bohm and D. Pines, Phys. Rev. **92**, 609 (1953).
[105] K. Kuroki, S. Onari, R. Arita, H. Usui, Y. Tanaka, H. Kontani, and H. Aoki, Phys. Rev. Lett. **101**, 087004 (2008).
[106] S. Graser, T. A. Maier, P. J. Hirschfeld, and D. J. Scalapino, New J. Phys. **11**, 025016 (2009).
[107] T. A. Maier, S. Graser, P. J. Hirschfeld, and D. J. Scalapino, Phys. Rev. B **83**, 100515(R) (2011).
[108] K. Nomura, S. Ryu, and D.-H. Lee, Phys. Rev. Lett. **103**, 216801 (2009).
[109] I. Žutić, J. Fabian, and S. Das Sarma, Rev. Mod. Phys. **76**, 323 (2004).
[110] S. Konschuh, Spin-orbit coupling effects: from graphene to graphite, Ph.D. thesis, University of Regensburg, 2011.
[111] M. Koshino and E. McCann, Phys. Rev. B **80**, 165409 (2009).
[112] A. Kormányos and G. Burkard, Phys. Rev. B **87**, 045419 (2013).
[113] Y.-Z. You and A. Vishwanath, npj Quantum Mater. **4**, 16 (2019).
[114] See Supplemental Material at http://link.aps.org/supplemental/10.1103/PhysRevLett.132.186401 for calculational details concerning the irreducible susceptibility χ^0, Γ vertex function, two-particle response function linear algebra, RPA, self-consistent Hartree-Fock treatment, as well as, details about the correlated low-energy band structures for different broken phases.